J Mater Sci (2009) 44:1868–1872
DOI 10.1007/s10853-008-3235-4

The morphotropic phase boundary and electrical properties of $(1 - x)Pb(Zn_{1/2}W_{1/2})O_3$–$xPb(Zr_{0.5}Ti_{0.5})O_3$ ceramics

O. Khamman · X. Tan · S. Ananta · R. Yimnirun

Received: 20 November 2008 / Accepted: 29 December 2008 / Published online: 3 February 2009

Abstract Ceramics in the solid solution of $(1 - x)Pb(Zn_{1/2}W_{1/2})O_3$–$xPb(Zr_{0.5}Ti_{0.5})O_3$ system, with $x = 0.80$, 0.85, 0.90, and 0.95, were synthesized with the solid-state reaction technique. The perovskite phase formation in the sintered ceramics was analyzed with X-ray diffraction. It shows that the rhombohedral and the tetragonal phases coexist in the ceramic with $x = 0.90$, indicating the morphotropic phase boundary (MPB) within this pseudo-binary system. Dielectric and ferroelectric properties measurements indicate that the transition temperature decreases while the remanent polarization increases with the addition of $Pb(Zn_{1/2}W_{1/2})O_3$. In the composition of $x = 0.85$ which is close to the MPB in the rhombohedral side, a high piezoelectric property with $d_{33} = 222$ pC/N was observed.

Introduction

Lead-containing perovskite ferroelectrics are of great importance to engineering technologies due to their unique dielectric and piezoelectric properties [1]. Lead zirconate titanate, $Pb(Zr_{1-y}Ti_y)O_3$, is the most studied system for piezoelectric applications in transducers and actuators [1–4]. The best piezoelectric properties are found in compositions close to the morphotropic phase boundary (MPB), roughly $Pb(Zr_{0.5}Ti_{0.5})O_3$ [1]. To further enhance their piezoelectric properties, other complex compounds have been incorporated into the $Pb(Zr_{0.5}Ti_{0.5})O_3$, such as $Pb(Ni_{1/3}Nb_{2/3})_3$ [5], $Pb(Zn_{1/3}Nb_{2/3})O_3$ [6], $Pb(Mg_{1/3}Nb_{2/3})O_3$ [7], and $Pb(Mg_{1/2}W_{1/2})O_3$ [8].

Lead zinc tungstate, $Pb(Zn_{1/2}W_{1/2})O_3$, is a complex perovskite compound with Zn^{2+} and W^{6+} ordered on the B-site of the ABO_3 perovskite lattice [9]. When cooling through the Curie temperature of 130 °C, it transforms from the cubic to a tetragonal structure. However, whether the tetragonal phase is ferroelectric or antiferroelectric is still unknown [9]. It should be noted that perovskite $Pb(Zn_{1/2}W_{1/2})O_3$ can only be synthesized under high pressure [10]. The conventional solid-state reaction method invariably leads to the mixture of Pb_2WO_5 and ZnO [11]. To the authors' knowledge, the complex perovskite $Pb(Zn_{1/2}W_{1/2})O_3$ has not been reported in literature to be incorporated into $Pb(Zr_{1-y}Ti_y)O_3$ for solid solutions. In addition to identifying the MPB and investigating the dielectric, piezoelectric, and ferroelectric properties in the $(1 - x)Pb(Zn_{1/2}W_{1/2})O_3$–$xPb(Zr_{0.5}Ti_{0.5})O_3$ solid solution system, the present study aims to determine the solubility limit of $Pb(Zn_{1/2}W_{1/2})O_3$ in $Pb(Zr_{0.5}Ti_{0.5})O_3$ and to explore if long range cation order can be developed in $Pb(Zr_{0.5}Ti_{0.5})O_3$-based solid solutions [8].

Experimental

Ceramics in the $(1 - x)Pb(Zn_{1/2}W_{1/2})O_3$–$xPb(Zr_{0.5}Ti_{0.5})O_3$ pseudo-binary system with $x = 0.80$, 0.85, 0.90, and 0.95 were prepared with a two-step reaction method. First, powders of $ZnWO_4$ and $ZrTiO_4$ were synthesized. The $ZnWO_4$ precursor was formed by reacting ZnO (99.9%) with WO_3 (99.9%) at 1000 °C for 4 h while the $ZrTiO_4$ precursor was formed by reacting ZrO_2 (99%) with TiO_2

O. Khamman · S. Ananta · R. Yimnirun
Department of Physics, Faculty of Science, Chiang Mai University, Chiang Mai 50200, Thailand

X. Tan (✉)
Department of Materials Science and Engineering, Iowa State University, Ames, IA 50011, USA
e-mail: xtan@iastate.edu

(99.9%) at 1400 °C for 4 h. Appropriate amount of $ZnWO_4$ and $ZrTiO_4$ were then mixed with PbO (99.9%, with 2 mol% excess) and milled, dried, and calcined at 900 °C for 4 h. The green compact of ceramics was formed by uniaxially pressing powders containing 2 wt% polyvinyl alcohol binder. Sintering was carried out at temperatures between 1100 and 1175 °C. To prevent PbO loss from the pellets, a PbO atmosphere was provided with a bed of $PbZrO_3$ powder placed in the vicinity of the pellets.

The density of the ceramics was measured by the Archimedes method, and the grain size was examined by scanning electron microscopy (SEM). The X-ray diffraction was used to verify the phase purity and determine the crystal structure. The ceramic pellets were polished and then electroded with gold for dielectric measurements. The samples were heated from room temperature at 2 °C/min for the measurement. For the piezoelectric measurement, samples were poled under 30 kV/cm for 10 min at 120 °C. The piezoelectric coefficient d_{33} was measured using a d_{33} meter 24 h after poling. The polarization hysteresis measurement was carried out with a standardized ferroelectric test system at room temperature with a frequency of about 4 Hz.

Results and discussion

The measured density of the sintered ceramic pellets in the pseudo-binary system $(1-x)Pb(Zn_{1/2}W_{1/2})O_3$–$xPb(Zr_{0.5}Ti_{0.5})O_3$ is listed in Table 1. The relative density for all the pellets was found to be above 90%. The addition of $Pb(Zn_{1/2}W_{1/2})O_3$ seems to enhance the sinterability of the solid solution ceramics. SEM micrographs of the fracture surfaces of the ceramic pellets are shown in Fig. 1. It can be seen that grains are uniform with clear grain boundaries. The average grain size determined from these micrographs is also listed in Table 1. Obviously, incorporating up to 10 mol% of $Pb(Zn_{1/2}W_{1/2})O_3$ into $Pb(Zr_{0.5}Ti_{0.5})O_3$ significantly increases the grain size. However, beyond 10 mol%, it appears to show the opposite effect.

X-ray diffraction patterns of the $(1-x)Pb(Zn_{1/2}W_{1/2})O_3$–$xPb(Zr_{0.5}Ti_{0.5})O_3$ solid solution ceramics are presented in Fig. 2. Within the detection limit of the diffractometer, sintered ceramics are phase pure with the perovskite structure with x down to 0.80. Further increase in $Pb(Zn_{1/2}W_{1/2})O_3$ content invariably leads to the formation of second phases. Therefore, the solubility limit of $Pb(Zn_{1/2}W_{1/2})O_3$ in $Pb(Zr_{0.5}Ti_{0.5})O_3$ is 20 mol%. Furthermore, the X-ray diffraction data in the range of 15–20° for 2θ (not shown in Fig. 2) did not display any diffraction intensity peak, suggesting the absence of long range cation order in these sintered ceramics [8].

Table 1 Characteristics of the sintered $(1-x)Pb(Zn_{1/2}W_{1/2})O_3$–$xPb(Zr_{0.5}Ti_{0.5})O_3$ ceramics

x	Relative density (%)	Grain size (μm)
0.80	95	11.5
0.85	92	28.5
0.90	91	41.8
0.95	90	20.8

Close examination indicates significant changes in the pseudo-cubic $(200)_c$ peak when composition varies, as marked with the dashed box in Fig. 2. For the composition of $x = 0.95$, the X-ray diffraction pattern shows an obvious $(200)_c$ peak splitting which is indicative of the tetragonal symmetry of the perovskite structure. As the $Pb(Zn_{1/2}W_{1/2})O_3$ content increases in the solid solution, the $(200)_c$ peak transforms to a single peak which suggests a rhombohedral distortion of the perovskite structure. The results show that a morphotropic phase boundary (MPB), separating the rhombohedral from the tetragonal phase, exists at $x = 0.90$ in the pseudo-binary $(1-x)Pb(Zn_{1/2}W_{1/2})O_3$–$xPb(Zr_{0.5}Ti_{0.5})O_3$ solid solution system. It is interesting to notice that the phase evolution sequence in the present $Pb(Zn_{1/2}W_{1/2})O_3$–$Pb(Zr_{0.5}Ti_{0.5})O_3$ system is very similar to that in the $Pb(Ni_{1/3}Nb_{2/3})O_3$–$Pb(Zr_{0.5}Ti_{0.5})O_3$ [5] and the $Pb(Zn_{1/3}Nb_{2/3})O_3$–$Pb(Zr_{0.5}Ti_{0.5})O_3$ systems [6].

The temperature dependence of dielectric constant ε_r and loss tangent $\tan\delta$ measured at 1 kHz for the ceramics are plotted in Fig. 3. It is shown that with increasing $Pb(Zn_{1/2}W_{1/2})O_3$ content in the $(1-x)Pb(Zn_{1/2}W_{1/2})O_3$–$xPb(Zr_{0.5}Ti_{0.5})O_3$ solid solution, the paraelectric–ferroelectric transition temperature T_m decreases continuously. Overall, all the ceramics show very high dielectric permittivity. The dielectric constant at T_m, denoted as ε_m hereafter, shows the highest value of 38410 in the composition of $x = 0.90$. This composition, as revealed by the X-ray diffraction patterns shown in Fig. 2, is the MPB composition. Therefore, the results from the dielectric measurement are in support of the x-ray diffraction data. The values of T_m and ε_m for the ceramic series are listed in Table 2 for clarity.

It is also noticed from Fig. 3 that the paraelectric–ferroelectric transition peak becomes broadened slightly with increasing $Pb(Zn_{1/2}W_{1/2})O_3$ content. In addition, a new dielectric anomaly emerges around 260 °C in the composition of $x = 0.80$. Detailed comparison of the dielectric constant under different measuring frequencies between compositions of $x = 0.80$ and 0.95 is shown in Fig. 4. A weak frequency dependence is seen in the dielectric constant.

The broadened dielectric peak suggests that the dielectric constant ε_r at temperatures above T_m should follow a general expression [5, 12]:

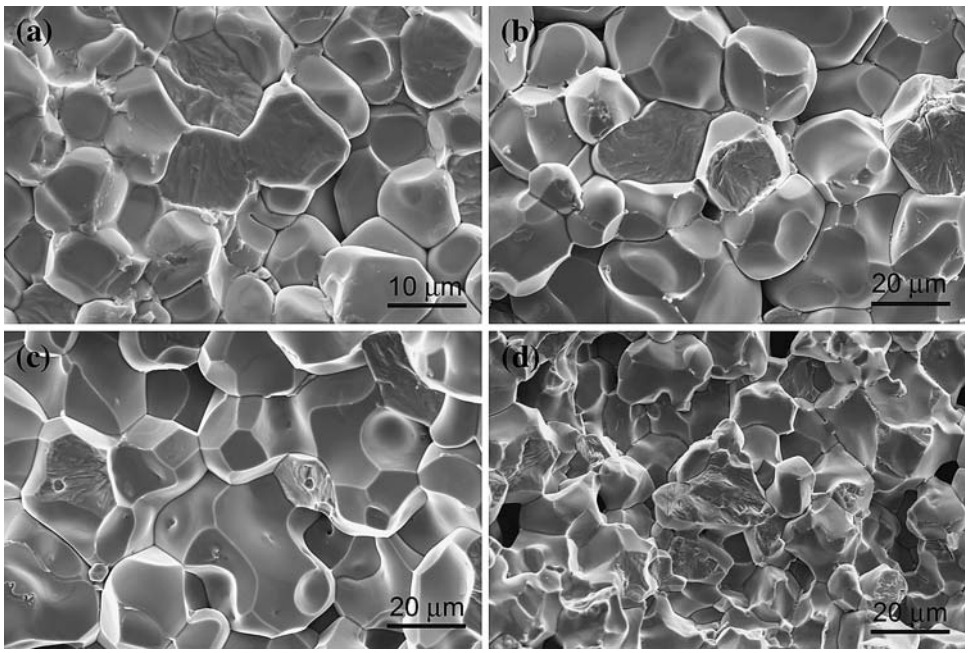

Fig. 1 SEM micrographs revealing the fracture surfaces of $(1 - x)Pb(Zn_{1/2}W_{1/2})O_3$–$xPb(Zr_{0.5}Ti_{0.5})O_3$ ceramics. **a** $x = 0.80$, **b** $x = 0.85$, **c** $x = 0.90$, **d** $x = 0.95$

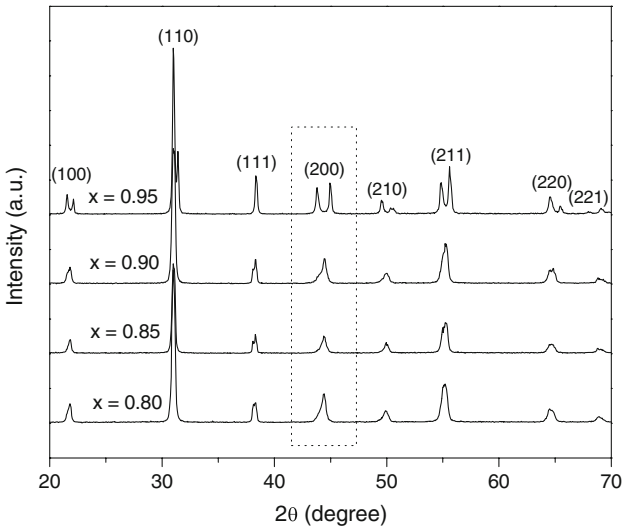

Fig. 2 X-ray diffraction spectra for the sintered $(1 - x)Pb(Zn_{1/2}W_{1/2})O_3$–$xPb(Zr_{0.5}Ti_{0.5})O_3$ ceramics. The intensity peaks are index with the pseudo-cubic perovskite structure. The $(200)_c$ peak in the dashed box reveals the change of distortion

$$\frac{\varepsilon_m}{\varepsilon_r} = 1 + \frac{[T - T_m]^\gamma}{2\delta^2} \quad (1)$$

where γ is a parameter indicating the degree of dielectric relaxation while the parameter δ can be used to evaluate the degree of the diffuseness of the phase transition. When $\gamma = 1$, Eq. 1 becomes the Curie–Weiss law, while for $\gamma = 2$ this equation becomes the quadratic relationship describing the classic relaxor ferroelectric $Pb(Mg_{1/3}Nb_{2/3})O_3$ [13]. According to Eq. 1, the values of ln $[(\varepsilon_m/\varepsilon_r) - 1]$ are plotted against ln $(T - T_m)$ in Fig. 5 for all the sintered

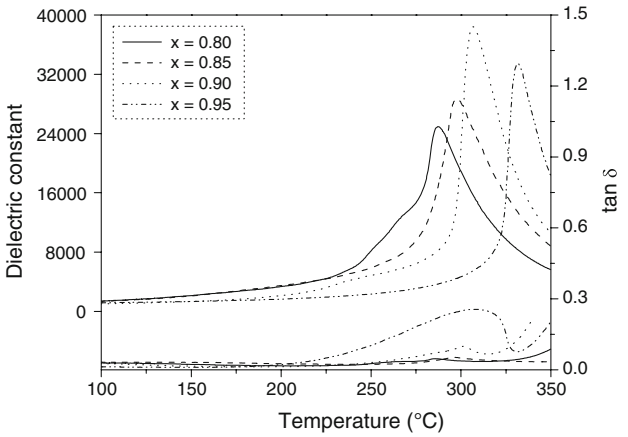

Fig. 3 Dielectric constant ε_r and loss tangent tan δ as a function of temperature measured at 1 kHz during heating in the $(1 - x)Pb(Zn_{1/2}W_{1/2})O_3$–$xPb(Zr_{0.5}Ti_{0.5})O_3$ ceramics

Table 2 Dielectric and piezoelectric properties of the $(1 - x)Pb(Zn_{1/2}W_{1/2})O_3$–$xPb(Zr_{0.5}Ti_{0.5})O_3$ ceramics

x	ε_m	T_m (°C)	γ	δ	d_{33} (pC/N)
0.80	24930	287	1.55	8.07	142
0.85	28730	297	1.55	7.50	222
0.90	38410	306	1.53	7.39	188
0.95	33480	331	1.43	6.13	136

ceramics, using the data obtained at 1 kHz. Remarkably good linearity within the measurement temperature range above T_m is evident. Using the intercept and the slope of the fitted lines in Fig. 5, γ and δ for each composition are determined and listed in Table 2. It is found that with

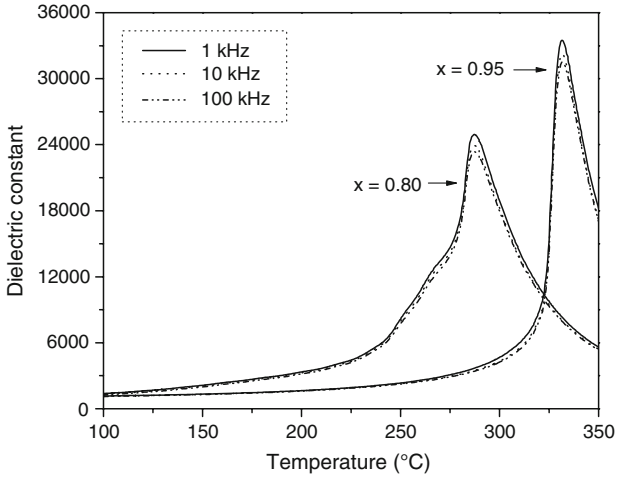

Fig. 4 Dielectric constant ε_r as a function of temperature measured at 1, 10, and 100 kHz during heating in the $0.20Pb(Zn_{1/2}W_{1/2})O_3$–$0.80Pb(Zr_{0.5}Ti_{0.5})O_3$ and the $0.05Pb(Zn_{1/2}W_{1/2})O_3$–$0.95Pb(Zr_{0.5}Ti_{0.5})O_3$ ceramics

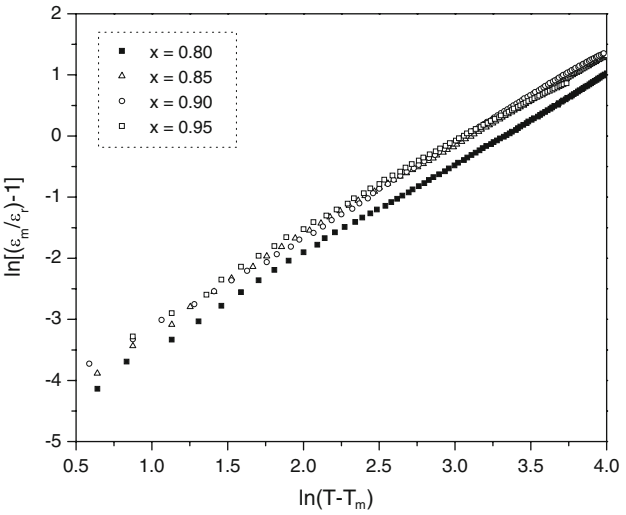

Fig. 5 The ln $[(\varepsilon_m/\varepsilon_r) - 1]$ vs. ln $(T - T_m)$ plot for the $(1 - x)Pb(Zn_{1/2}W_{1/2})O_3$–$xPb(Zr_{0.5}Ti_{0.5})O_3$ ceramics

increasing amount of $Pb(Zn_{1/2}W_{1/2})O_3$ in the $(1 - x)Pb(Zn_{1/2}W_{1/2})O_3$–$xPb(Zr_{0.5}Ti_{0.5})O_3$ solid solution, both the relaxation parameter γ and the diffuseness parameter δ increases. This is indicative of an increasing degree of disorder of the electrical dipole moments in the solid solution ceramics.

The piezoelectric property of the poled ceramics was measured at room temperature with a quasi-static d_{33} meter and is also listed in Table 2. The highest d_{33} value (222 pC/N) is found in the ceramic of $0.15Pb(Zn_{1/2}W_{1/2})O_3$–$0.85Pb(Zr_{0.5}Ti_{0.5})O_3$, a composition close to the MPB in the rhombohedral side. Optimizing processing conditions is expected to further increase the piezoelectric property.

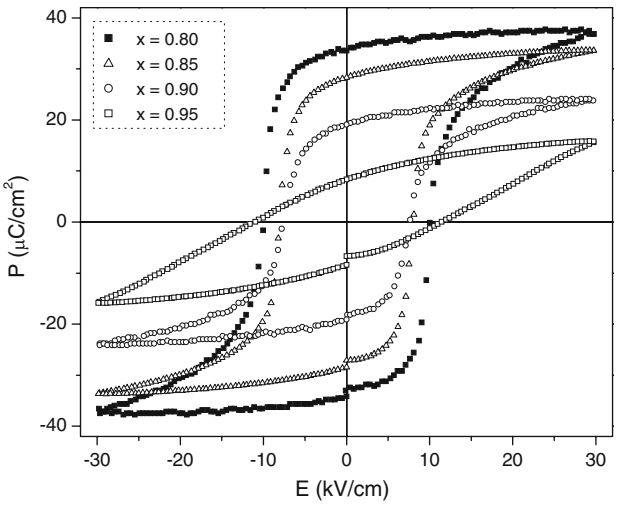

Fig. 6 Polarization versus electric field hysteresis loops measured at room temperature at 4 Hz in the $(1 - x)Pb(Zn_{1/2}W_{1/2})O_3$–$xPb(Zr_{0.5}Ti_{0.5})O_3$ ceramics

Finally, the ferroelectric properties of the sintered ceramics were evaluated with the electrical polarization versus field hysteresis loop measurements. As shown in Fig. 6, all samples exhibit a profound hysteretic behavior. In the ceramic of $0.05Pb(Zn_{1/2}W_{1/2})O_3$–$0.95Pb(Zr_{0.5}Ti_{0.5})O_3$, a non-saturated hysteresis loop is observed at a peak electric field of 30 kV/cm. However, saturated loops are seen in ceramics with a higher content of $Pb(Zn_{1/2}W_{1/2})O_3$. In addition, the remanent polarization P_r is observed to increase dramatically with increasing $Pb(Zn_{1/2}W_{1/2})O_3$ content. In the ceramic with composition of $x = 0.80$, P_r reached 33.6 μC/cm^2. The shape of the ferroelectric hysteresis loop can be quantitatively assessed with the so-called squareness parameter R_{sq}, defined previously in literature [14]:

$$R_{sq} = \left(\frac{P_r}{P_s}\right) + \left(\frac{P_{1.1E_c}}{P_r}\right) \quad (2)$$

where P_s is the saturation polarization, E_c is the coercive field, $P_{1.1E_c}$ is the polarization at the field of $1.1E_c$. For a perfect square loop, R_{sq} is equal to 2.00. With the data presented in Fig. 6, the loop squareness parameter R_{sq} is calculated. The result is listed in Table 3, together with the remanent polarization P_r and the coercive field E_c. Incorporating $Pb(Zn_{1/2}W_{1/2})O_3$ obviously enhances the ferroelectric properties significantly.

Conclusions

Phase pure perovskite ceramics in the $(1 - x)Pb(Zn_{1/2}W_{1/2})O_3$–$xPb(Zr_{0.5}Ti_{0.5})O_3$ system can be prepared with the solid-state reaction method with up to 20 mol% of

Table 3 Ferroelectric properties of the $(1 - x)Pb(Zn_{1/2}W_{1/2})O_3$–$xPb(Zr_{0.5}Ti_{0.5})O_3$ ceramics

x	P_r (μC/cm^2)	E_c (kV/cm)	R_{sq}
0.80	33.6	10.1	1.24
0.85	28.4	8.2	1.36
0.90	19.2	7.8	1.20
0.95	8.4	11.4	0.66

$Pb(Zn_{1/2}W_{1/2})O_3$. In the composition range for a stable perovskite structure, the MPB composition is identified at $x = 0.90$. This MPB separates the tetragonal phase from the rhombohedral phase. At the MPB composition, a remarkably high dielectric constant ε_m of 38410 is observed at the ferroelectric transition temperature T_m. In the ceramic of $0.15Pb(Zn_{1/2}W_{1/2})O_3$–$0.85Pb(Zr_{0.5}Ti_{0.5})O_3$, a composition in the rhombohedral side of MPB, the best piezoelectric property ($d_{33} = 222$ pC/N) is detected. Furthermore, the addition of $Pb(Zn_{1/2}W_{1/2})O_3$ in $Pb(Zr_{0.5}Ti_{0.5})O_3$ dramatically enhances the ferroelectric properties, manifested by the large increase in the remanent polarization and the hysteresis loop squareness parameter. Therefore, the $(1 - x)Pb(Zn_{1/2}W_{1/2})O_3$–$xPb(Zr_{0.5}Ti_{0.5})O_3$ solid solution offers a new material system for various device applications.

Acknowledgements This work was supported by the National Science Foundation through the CAREER grant DMR-0346819 and the Thailand Research Fund (TRF), the Commission on Higher Education (CHE), and the Faculty of Science, Chiang Mai University, Thailand.

References

1. Jaffe B, Cook WR, Jaffe H (1971) Piezoelectric ceramics. Academic Press, London
2. Haertling GH (1999) J Am Ceram Soc 82:797
3. Cross LE (1996) Mater Chem Phys 43:108
4. Uchino K (2000) Ferroelectric devices. Marcel Dekker, Inc, New York
5. Vittayakorn N, Rujijanagul G, Tan X, Marquardt MA, Cann DP (2004) J Appl Phys 96:5103
6. Vittayakorn N, Rujijanagul G, Tan X, He H, Marquardt MA, Cann DP (2006) J Electroceram 16:141
7. Yimnirun R, Ananta S, Laoratanakul P (2005) J Eur Ceram Soc 25:3235
8. White D, Zhao X, Besser MF, Tan X (2008) J Mater Sci 43:5258. doi:10.1007/s10853-008-2772-1
9. Okai B, Yoshimoto J, Fujita T (1974) J Phys Soc Jpn 37:281
10. Fujita T, Fukunaga O, Nakagawa T, Nomura S (1970) Mater Res Bull 5:759
11. Lee WJ, Kim NK (2008) J Mater Sci 43:3608. doi:10.1007/s10853-008-2574-5
12. Uchino K, Nomura S (1982) Ferroelectr Lett 44:55
13. Smolenskii GA (1970) J Phys Soc Jpn 28(Suppl):26
14. Jin B, Kim J, Kim SC (1997) Appl Phys A 65:53